THE JOURNAL OF BIOLOGICAL CHEMISTRY VOL. 290, NO. 43, pp. 26088–26102, October 23, 2015

A Role for Widely Interspaced Zinc Finger (WIZ) in Retention of the G9a Methyltransferase on Chromatin*

Received for publication, March 24, 2015, and in revised form, August 23, 2015 Published, JBC Papers in Press, September 3, 2015, DOI 10.1074/jbc.M115.654459

Jeremy M. Simon[‡], Joel S. Parker[§], Feng Liu[¶], Scott B. Rothbart[‖], Slimane Ait-Si-Ali[**], Brian D. Strahl[‡‡], Jian Jin[§§], Ian J. Davis[¶¶], Amber L. Mosley[‖‖], and Samantha G. Pattenden[¶1]

From the [‡]Carolina Institute for Developmental Disabilities, Department of Cell Biology and Physiology, and the Department of Genetics, Curriculum in Bioinformatics and Computational Biology, Lineberger Comprehensive Cancer Center, University of North Carolina at Chapel Hill, Chapel Hill, North Carolina 27599, the [§]Department of Genetics and the Lineberger Comprehensive Cancer Center, University of North Carolina at Chapel Hill, Chapel Hill, North Carolina 27599, the [¶]Center for Integrative Chemical Biology and Drug Discovery, Eshelman School of Pharmacy, University of North Carolina, Chapel Hill, Chapel Hill, North Carolina 27599, the [‖]Center for Epigenetics, Van Andel Research Institute, Grand Rapids, Michigan 49503, the [**]Laboratoire Epigénétique et Destin Cellulaire, UMR7216, CNRS, Université Paris Diderot, Sorbonne Paris Cité, 75013 Paris, France, the [‡‡]Lineberger Comprehensive Cancer Center, the Curriculum in Genetics and Molecular Biology, and the Department of Biochemistry and Biophysics, University of North Carolina at Chapel Hill, Chapel Hill, North Carolina 27599, the [§§]Department of Structural and Chemical Biology, the Department of Oncological Sciences, and the Department of Pharmacology and Systems Therapeutics, Icahn School of Medicine at Mount Sinai, New York, New York 10029, the [¶¶]Department of Genetics, the Lineberger Comprehensive Cancer Center, the Department of Pediatrics, and the Carolina Center for Genome Sciences, University of North Carolina at Chapel Hill, Chapel Hill, North Carolina 27599, and the [‖‖]Department of Biochemistry and Molecular Biology and the Center for Computational Biology and Bioinformatics, Indiana University School of Medicine, Indianapolis, Indiana 46202

Background: G9a-GLP lysine methyltransferases mono- and di-methylate histone H3 lysine 9 (H3K9me2).
Results: Widely interspaced zinc finger (WIZ) regulates H3K9me2 levels through a mechanism that involves retention of G9a on chromatin.
Conclusion: The G9a-GLP-WIZ complex has unique functions when bound to chromatin that are independent of the H3K9me2 mark.
Significance: Combining pharmacologic and genetic manipulations is essential to any translational hypotheses related to G9a function.

G9a and GLP lysine methyltransferases form a heterodimeric complex that is responsible for the majority of histone H3 lysine 9 mono- and di-methylation (H3K9me1/me2). Widely interspaced zinc finger (WIZ) associates with the G9a-GLP protein complex, but its role in mediating lysine methylation is poorly defined. Here, we show that WIZ regulates global H3K9me2 levels by facilitating the interaction of G9a with chromatin. Disrupting the association of G9a-GLP with chromatin by depleting WIZ resulted in altered gene expression and protein-protein interactions that were distinguishable from that of small molecule-based inhibition of G9a/GLP, supporting discrete functions of the G9a-GLP-WIZ chromatin complex in addition to H3K9me2 methylation.

The posttranslational modification of the N-terminal lysines of histone proteins is associated with diverse biological consequences including changes in transcription and chromatin architecture. Lysine methylation is commonly performed by the SET (Su(var)3–9-Enhancer of *zeste*-Trithorax) domain-containing proteins (1–5). Two important members of this family are the G9a (EHMT2) and GLP[2] (EHMT1) lysine methyltransferases. These enzymes are implicated in a variety of disease and biological processes (6); they demonstrate both co-activator and co-repressor functions (6–8) and interact with other SET domain-containing proteins including SETDB1, Suv39H1, and the PRC2 complex (9, 10). G9a and GLP show similar substrate specificities (11–13); they methylate histones H1 (11, 12, 14), H3K27 (11, 15) and H3K56 (16), as well as a number of non-histone proteins (17–21), but are best characterized as the major lysine methyltransferases involved in mono- and di-methylation of H3K9 (11, 22–25).

Transcriptional silencing and the H3K9 mono- and di-methylation functions of G9a and GLP are dependent on heterodimerization through their respective SET domains (25). Studies in mouse *G9a* and *Glp* knock-out cells demonstrate that loss of either G9a or GLP results in degradation of the remaining protein partner (13, 25). Reconstitution of these cells with a heteromeric complex consisting of either a G9a or a GLP catalytic mutant suggests that the catalytic activity

* This work was supported, in whole or in part, by National Institutes of Health Grants CA181343 (to S. B. R.), R01GM110058 (to B. D. S.), R01CA166447 (to I. J. D), and R01GM103893 (to J. J.). This work was also supported by the W. M. Keck Foundation (to B. D. S.). The authors declare that they have no conflicts of interest with the contents of this article.
[1] Supported by National Institutes of Health Grant R01GM100919 from NIGMS (awarded to Dr. Stephen Frye) and by the Carolina Partnership and the University Cancer Research Fund, University of North Carolina at Chapel Hill. To whom correspondence should be addressed: Ctr. for Integrative Chemical Biology and Drug Discovery, Eshelman School of Pharmacy, University of North Carolina at Chapel Hill, Marsico Hall, 125 Mason Farm, Chapel Hill, NC 27599. Tel.: 919-843-0766; Fax: 919-843-8465; E-mail: pattenden@unc.edu.

[2] The abbreviations used are: GLP, G9a-like protein; WIZ, widely interspaced zinc finger; DMSO, dimethyl sulfoxide; qPCR, quantitative PCR; IP, immunoprecipitation; CTCF, CCCTC-binding factor; SAINT, significance analysis of interactome; CHX, cycloheximide; TSS, transcription start site.

of GLP, but not G9a, is dispensable for H3K9 methylation (13).

Although the interaction between G9a and GLP has been studied extensively, the interaction between these proteins and a third complex member, widely interspaced zinc finger (WIZ) protein, is less well understood. The mouse *Wiz* gene products were identified as two alternatively spliced isoforms, *WizS* and *WizL*, which were abundantly expressed in the brain compared with other tissue types (26). WIZ has C_2H_2-type zinc finger motifs, originally characterized in the *Xenopus* TFIIIA (27) and *Drosophila* Krüppel transcription factors (28). Typical C_2H_2-type zinc finger motifs are separated by seven amino acids. The WIZ zinc fingers are widely spaced, being separated by distances ranging from 16 to 258 amino acids in mouse (26) and from 16 to 263 amino acids in the longest human splice variant. Mutational analysis has demonstrated that WIZ interacts with the C-terminal SET domain of G9a or GLP through its C-terminal zinc finger (29). WIZ has been shown to bridge the interaction between G9a-GLP and the transcriptional co-repressors C-terminal binding protein 1 (CtBP1) and CtBP2, possibly to help recruit G9a-GLP to specific genomic loci (29), and is a non-histone methylation target for G9a (18).

WIZ has also been implicated in G9a and GLP protein stability (29). We found that *WIZ* knockdown leads to an H3K9me2 loss that is not attributable to the degradation of G9a or GLP protein; rather, WIZ is important for the retention of G9a on chromatin. Using pharmacological inhibition of G9a and gene-silencing methods to regulate *WIZ*, we compared G9a localization with evidence of enzymatic activity. Although the loss of G9a chromatin localization mediated by WIZ and small molecule inhibition of G9a and GLP activity (30) both resulted in a loss of H3K9me2, these treatments variably affected gene expression and G9a protein-interacting partners.

Experimental Procedures

Cell Culture—HEK293T cells were grown in DMEM supplemented with 10% FBS. FLAG-HA-G9a HeLa cells (9) were grown in MEM supplemented with 5% FBS and 5% horse serum. Stable pools of *WIZ* shRNA knockdown and control shRNA knockdown cells were created as follows. FLAG-HA-G9a HeLa cells (9) were transduced with lentivirus containing *WIZ* shRNA with a target sequence identical to the *WIZ* siRNA used in this study (Sigma Mission WIZ, SHCLNV; clone ID TRCN0000253784) or a control shRNA that contains an shRNA insert that does not target any known genes from any species (Sigma Mission pLKO.1-puro non-target shRNA, SHC016V). Transduced cells were selected with 5 μg/ml puromycin, and the resulting stable pools were grown in MEM supplemented with 5% FBS, 5% horse serum, and 5 μg/ml puromycin.

WIZ Cloning—*WIZ* cDNA (Thermo Fisher Scientific MH51768-101549168) was PCR-amplified with o-WIZclone-1 (forward, 5′-GGGTCTAGAGATGGTGGCCATGGACTTGGG-3′) and o-WIZclone-2 (reverse, 5′-GCGCCGCGGGGGAGCCTCTGCCGCCGCTG-3′) and cloned into pcDNA™3.1/*myc*-His B (Invitrogen, V855-20) with XbaI and SacII.

siRNA Knockdown and Compound Treatment—Cells were treated with the indicated media supplemented with 1 μM UNC0638 (30) or the volume equivalent of DMSO for 48 or 96 h, as indicated. All siRNAs were purchased from GE Healthcare Dharmacon, and transfections were performed as per the manufacturer's instructions with DharmaFECT 4 transfection reagent. siRNAs used in this study were as follows: control (scrambled) siRNA (Dharmacon non-targeting 001810-04), G9a siRNA (Dharmacon 006937-05), and *WIZ* siRNA custom (ON-TARGET*plus*, Dharmacon) with sense sequence 5′-CAGCAGAGGUCAAGGCCAAUU-3′ and antisense sequence 5′-UUGGCCUUUGACCUCUGCUGUU-3′.

Quantitative RT-PCR—RNA was extracted using the RNeasy Plus mini kit (Qiagen), and RNA was quantified on a NanoDrop 2000 spectrophotometer (Thermo Fisher Scientific). The reverse transcription reaction was performed with 500 ng of RNA using Superscript III First Strand Synthesis Supermix (Invitrogen 1172-050) according to the manufacturer instructions. The resulting cDNA was diluted 1:10, and 2 μl of the mixture was used for each PCR reaction. Quantitative PCR was performed using Roche FastStart Universal SYBR Green Master Mix (Roche Applied Science) in a 384-well plate format on an ABI 2900HT instrument. Oligo sequences are available upon request.

Immunoprecipitation—Whole cell protein extract was prepared by lysing cells in Cytobuster™ protein extraction reagent (EMD Millipore 71009) supplemented with 25 units of Benzonase nuclease (EMD Millipore 101654). Subcellular fractionation was performed using the Pierce Subcellular Fractionation Kit (Thermo Fisher Scientific 78840) according to the manufacturer's instructions. FLAG-HA-G9a was immunoprecipitated from the samples described with Anti-FLAG® M2 affinity gel (Sigma A2220) overnight at 4 °C and washed three times in TBST (20 mM Tris-HCl, pH 8.0, 150 mM NaCl, and 0.1% Tween 20). Bound proteins were eluted by boiling in 1× SDS-PAGE loading buffer and subjected to Western blot analysis.

G9a Protein Stability Assay—FLAG-HA-G9a cells were plated on 6-well plates at a density of 5×10^5 cells/well. After 24 h, cells were transfected with siRNA as described previously or treated with 1 μM UNC0638 (or volume equivalent of DMSO) and incubated for 48 h. Cells were then treated with 1 μM MG132 (or volume equivalent of DMSO) for 12 h followed by the addition of 25 μg/ml (Fig. 3*A*) or 50 μg/ml (Fig. 3*B*) cycloheximide (or volume equivalent of ethanol) for 0, 4, 6, 9, or 13.5 h. Cells were lysed in Cytobuster™ protein extraction reagent (EMD Millipore 71009) supplemented with 25 units of Benzonase nuclease (EMD Millipore 101654). The protein extract concentration was determined with Bradford reagent (Bio-Rad 500-0006) and a standard curve generated by known quantities of bovine serum albumin. Ten μg of lysate was run on SDS-PAGE and subjected to Western blotting.

Western Blotting and Densitometry—Western blotting was performed using a Typhoon imager (GE Healthcare) as described elsewhere (31) or using a LI-COR Odyssey as described elsewhere (32). Densitometry was performed using ImageJ software or LI-COR Image Studio software.

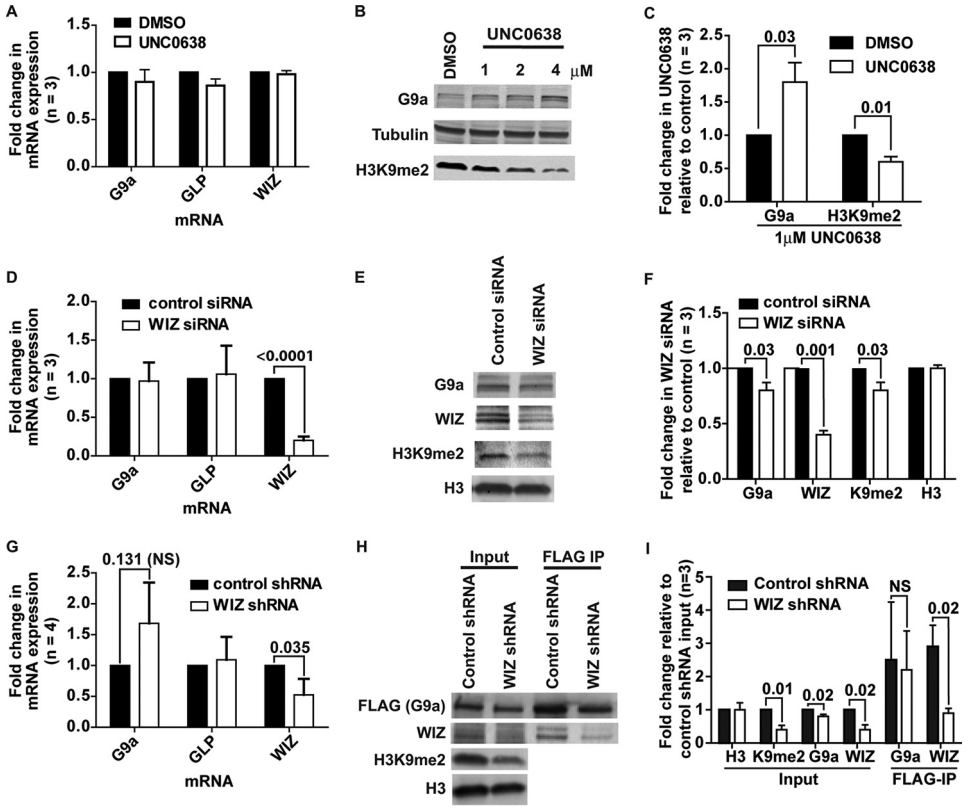

FIGURE 1. **Treatment with UNC0638 and knockdown of *WIZ* results in loss of H3K9me2.** *A*, RT-qPCR of *G9a*, *GLP*, and *WIZ* mRNA expression in HEK293T cells treated with UNC0638 or vehicle control for 48 h, normalized to *B2M* expression. *Error bars* represent the standard deviation of three biological replicates. *B*, Western blots of whole cell extract from HEK293T cells treated with 1, 2, and 4 μM UNC0638 or vehicle control for 48 h. *C*, densitometry of Western blot bands represented by *B*. *Error bars* represent the standard deviation of three biological replicates. The *x* axis shows the G9a and H3K9me2 signals. The *y* axis shows the -fold change in densitometry signal after 1 μM UNC0638 treatment relative to DMSO. *p* values are indicated. *D*, RT-qPCR showing mRNA levels in HEK293T cells treated with control or *WIZ* siRNA for 48 h, normalized to *B2M* mRNA levels. *Error bars* represent the standard deviation of three biological replicates. *p* value is indicated. *E*, Western blots of whole cell extract from HEK293T cells treated with control or *WIZ* siRNA for 48 h. *F*, densitometry of Western blot bands represented in *E*. *Error bars* represent the standard deviation of three biological replicates. The *x* axis shows the G9a, WIZ, H3K9me2, and H3 signals. The *y* axis shows the -fold change in densitometry signal of *WIZ* siRNA knockdown relative to control. *p* values are indicated. *G*, RT-qPCR showing mRNA levels in HeLa FLAG-HA-G9a cells stably transfected with control or *WIZ* shRNA, normalized to *B2M* mRNA levels. *Error bars* represent the standard deviation of four biological replicates. *p* values are indicated. *NS*, no significant difference. *H*, Western blots of whole cell extract and FLAG IP from HeLa FLAG-HA-G9a cells stably transfected with control or *WIZ* shRNA. *I*, densitometry of Western blot bands represented in *H*. *Error bars* represent the standard deviation of three biological replicates. The *x* axis shows the input and G9a-FLAG IP signals for the indicated antibody. The *y* axis shows the -fold change in *WIZ* shRNA densitometry signal relative to control input signal. *p* values are indicated. *NS*, not significant.

Chromatin Immunoprecipitation—Chromatin immunoprecipitation was performed using the ChIP-IT High Sensitivity kit (Active Motif 53040) according to the manufacturer's instructions, except that the input samples were purified by phenol: chloroform extraction. The following antibodies were used: anti-H3K9me2 (Abcam ab1220), anti-H3K9me3 (Abcam ab8898), anti-G9a (Abcam ab40542), and Rabbit IgG (Jackson ImmunoResearch 011-000-003). ChIP samples were quantitated using the Qubit 2.0 fluorometer (Invitrogen). A portion of each sample was confirmed by qPCR as described above. The fold change over background was calculated using the ΔΔCt method (33), where immunoprecipitation (IP)/input for the ChIP antibody signal was compared with the IP/input value for IgG (background). After a confirmation of the ChIP signal over background, the remainder of the sample was submitted for high-throughput sequencing. Oligo sequences are available upon request.

High-throughput Sequencing and Data Analysis—Libraries were prepared for high-throughput using the Illumina TruSeq kit as per the manufacturer's recommendations. Single-end 50-bp reads were sequenced on an Illumina HiSeq. Reads were checked to be of sufficient quality, filtered to remove those with a significant adapter contribution using TagDust (34), and aligned to the reference human genome (hg19) using Bowtie (35). Regions of significant ChIP enrichment relative to input control ("peaks") were identified using MACS2, assuming fragments were 250 bp in length. Heat maps were generated in MATLAB by plotting the normalized ChIP-seq signal around the midpoints (±2 kb) of the union set of G9a peaks. Changes in the ChIP signal were illustrated by taking the arithmetic difference between treated and untreated samples. ChIP-seq data are available from NCBI Gene Expression Omnibus (accession number GSE67317). Genomic distributions were computed using CEAS (36). The CCCTC-binding factor (CTCF) and H3K4me3 ChIP-seq data from 293T cells were mined from BAM files provided by ENCODE (37). To find regions with significantly altered ChIP-seq enrichment, the number of overlapping aligned reads for all 500-bp non-overlapping windows across the genome was first tabulated for all samples. Only those windows with an average number of aligned reads exceeding 10 were retained. A binomial test was then applied to compare the G9a ChIP-seq signal between control

siRNA-treated and *WIZ* siRNA-treated cells at each of these windows; *p* values were corrected for multiple testing using the *q* value. Windows with $q < 1 \times 10^{-5}$ were retained and used for subsequent analyses.

Gene Expression Microarrays—RNA was extracted using the RNeasy Plus mini kit (Qiagen) and quantified on the Qubit fluorometer (Invitrogen). RNA quality was verified on an Agilent bioanalyzer before hybridization to human 8 × 60 K arrays (Agilent Technologies 28004). After scanning, microarray images were processed using Agilent Feature Extraction software according to the manufacturer-supplied protocols. The resulting background-subtracted and local regression (LOESS)-normalized log ratio data were collected and filtered to remove data generated from poor quality or low intensity spots. Probes with >30% missing data were removed from further evaluation. Dye swap replicates were inverted to match the log ratio direction of non-dye swap replicates. The remaining missing data were then imputed using weighted K-nearest neighbors (KNNimpute) (38). Testing for differential expression was performed using the statistical analysis of microarray (SAM) (39) one-class option for a comparison with DMSO or scrambled siRNA control and the two-class unpaired option when comparing UNC0638 with *WIZ* siRNA knockdown. A conservative false discovery rate threshold of 0.5% was set to identify differentially expressed genes in both experiments. The differential expression results were visualized using hierarchical cluster analysis based on average linkage clustering and a Pearson correlation distance metric. All statistical analyses were carried out using the R package (v3.1.1). Expression data are available from NCBI Gene Expression Omnibus (accession number GSE70914).

G9a Purification for Proteomics—G9a was purified from the HeLa FLAG-HA-G9a cell line (9) grown in a volume of 5 liters (~8 ml cell pellet), treated with either 1 μM UNC0638 or volume equivalent of DMSO for 48 h. Cells were centrifuged, washed once in PBS, and then frozen at −80 °C prior to purification. Purification was performed as follows. All buffers were supplemented with 1× protease inhibitor mixture (Roche 05056489001). Cell pellets were thawed on ice, resuspended in 40 ml of nuclei prep buffer (50% glycerol, 0.5% Nonidet P-40, 1 mM PMSF, 10 mM Tris-HCl, pH 7.4, 10 mM NaCl, and 3 mM $MgCl_2$), and incubated on ice for 10 min or until the nuclei were visible with trypan blue stain. Nuclei were pelleted, washed once with reticulocyte standard buffer (RSB: 10 mM Tris-HCl, pH 7.4, 10 mM NaCl, and 3 mM $MgCl_2$), resuspended in 24 ml of nuclei lysis buffer (0.2% Triton X-100, 20 mM HEPES, pH 7.9, 1.5 mM $MgCl_2$, 0.56 M NaCl, 10 mM KCl, and 0.5 mM DTT) supplemented with 250 units of Benzonase nuclease (EMD Millipore 101654), and incubated at 37 °C for 10 min followed by 1 h at 4 °C. The nuclear lysate was clarified by ultracentrifugation for 30 min at 40,000 rpm in a Ti70.1 rotor, and the salt concentration was lowered from ~0.42 to ~0.3 M with no salt nuclei lysis buffer (10 mM HEPES, pH 7.9, 1.5 mM $MgCl_2$, 10 mM KCl, and 0.5 mM DTT) followed by ultracentrifugation as described above. Lysate was transferred to a chromatography column (Bio-Rad 731-1550), and anti-FLAG® M2 affinity gel (Sigma A2220) equilibrated in 0.42 M NaCl nuclei lysis buffer (~100 μl of beads) was incubated with the clarified lysate overnight at 4 °C. Beads were washed with 50 ml of wash buffer (0.2% Triton X-100, 10 mM HEPES, pH 7.9, 1.5 mM $MgCl_2$, 0.3 M NaCl, and 10 mM KCl) and transferred to a 0.8-ml chromatography spin column (Pierce 89868). The protein was eluted by rotation at room temperature in 200 μl of elution buffer (50 mM Tris-HCl, pH 7.5, 0.5% Nonidet P-40, 0.15 M NaCl, and 0.2 mg/ml 2× FLAG peptide) three times for a total of ~600 μl of eluate. Eluates were diluted to 1.5 ml final volume in wash buffer and transferred to a chromatography column (Bio-Rad 732-6008). Anti-HA-agarose (Sigma A2095) was equilibrated in wash buffer (~100 μl beads) and incubated with the eluates overnight at 4 °C. Beads were washed with 30 ml of wash buffer and then transferred to a 0.8-ml chromatography spin column (Pierce 89868). Proteins were eluted in 200 μl of elution buffer (50 mM Tris-HCl, pH 7.5, 0.5% Nonidet P-40, 0.15 M NaCl, and 1.0 mg/ml HA peptide) four times for a total of ~800 μl of eluate. A portion of the eluates was visualized by silver staining, and the remaining sample was submitted for mass spectrometry analysis.

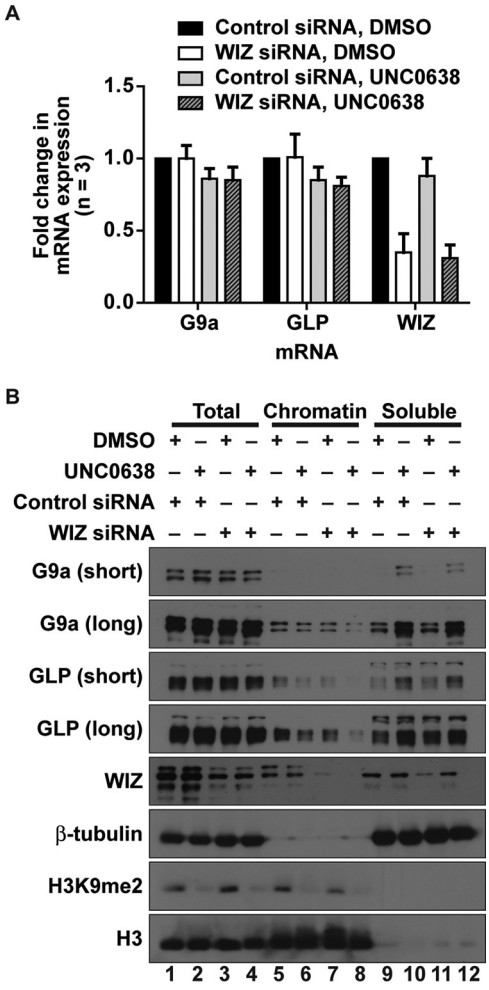

FIGURE 2. **A combination of enzymatic inhibition and reduction in WIZ protein levels has an additive effect on G9a chromatin localization.** *A*, RT-qPCR showing *G9a*, *GLP*, and *WIZ* mRNA levels in HEK293T cells treated with control or *WIZ* siRNA in combination with vehicle (DMSO) or 1 μM UNC0638 for 48 h. *Error bars* represent the standard deviation of three biological replicates. *B*, Western blots of fractionated lysates from HEK293T cells treated with control or *WIZ* siRNA in combination with vehicle (DMSO) or 1 μM UNC0638 for 48 h. The fractions are total (input), chromatin, and soluble.

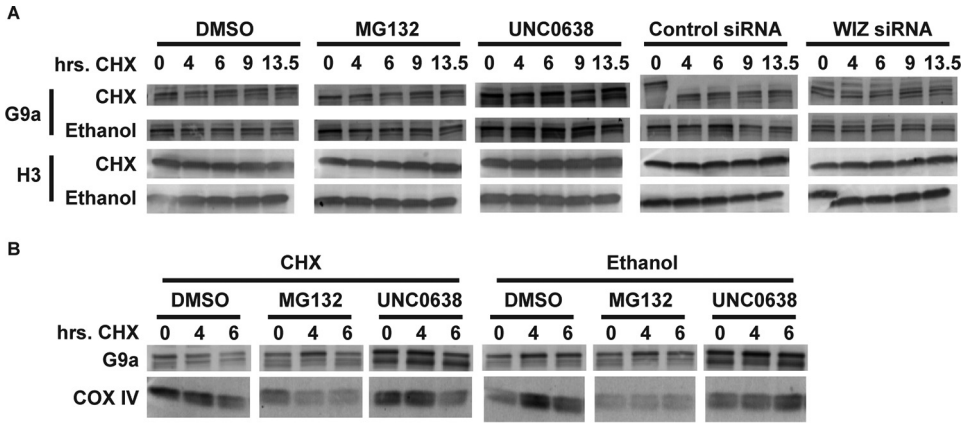

FIGURE 3. **UNC0638 treatment increases G9a protein levels but does not affect protein stability.** *A*, HeLa FLAG-HA-G9a cells were treated with vehicle control (DMSO), 1 μM UNC0638, *WIZ* siRNA, or control siRNA for 48 h or with 1 μM MG132 for 12 h followed by 50 μg/ml CHX or vehicle control (ethanol) for the indicated time. Whole cell extracts were Western-blotted with antibody against G9a or histone H3. *B*, G9a protein levels were assessed by Western blot following treatment with an inhibitor of *de novo* protein synthesis, CHX, in the presence of the MG132 proteasome inhibitor UNC0638 or *WIZ* siRNA knockdown. HeLa FLAG-HA-G9a cells were treated with vehicle control (DMSO) or 1 μM UNC0638 for 48 h or with 1 μM MG132 for 12 h followed by 25 μg/ml CHX or vehicle control (ethanol) for the indicated time. Whole cell extracts were Western-blotted with antibody against G9a or COXIV.

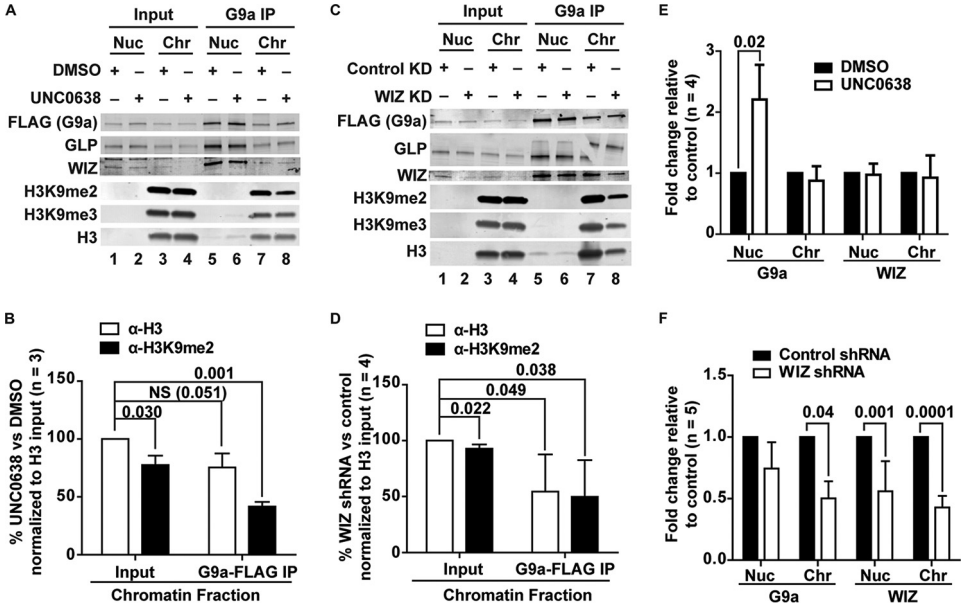

FIGURE 4. ***WIZ* shRNA knockdown decreases the association of G9a with chromatin.** *A*, Western blot of nuclear soluble (*Nuc*) and chromatin (*Chr*) fractions from HeLa FLAG-HA-G9a cells treated with vehicle (DMSO) or 1 μM UNC0638 for 48 h. FLAG-HA-G9a was immunoprecipitated with FLAG-agarose (Sigma). *B*, densitometry of Western blot bands from the chromatin fraction represented by *A*. *Error bars* represent the standard deviation of three biological replicates. The *x* axis shows the input and G9a-FLAG IP signals. The *y* axis shows the percent densitometry signal, which was calculated by normalizing H3K9me2 band density to the respective UNC0638 or DMSO H3 input signal and then dividing UNC0638-treated by DMSO-treated band densities. *p* values are indicated. *NS*, not significant. *C*, Western blot of nuclear soluble and chromatin fractions from HeLa FLAG-HA-G9a cells stably expressing control or *WIZ* shRNA knockdowns. FLAG-HA-G9a was immunoprecipitated with FLAG-agarose (Sigma). *D*, densitometry of Western blot bands from the chromatin fraction represented by *C*. *Error bars* represent the standard deviation of four biological replicates. The *x* axis shows the input and G9a-FLAG IP signals. The *y* axis shows the percent densitometry signal, which was calculated as described for *B*. *p* values are indicated. *E*, densitometry of Western blot bands represented by the input samples shown in *A*. The *y* axis shows the -fold change in signal from cells treated with UNC0638 compared with those treated with DMSO. The *x* axis shows the G9a or WIZ signal from the nuclear soluble or chromatin fractions. *Error bars* represent the average of four biological replicates. *p* values are indicated. *F*, densitometry of Western blot bands represented by the input samples in *C* as described for *E*, except *error bars* represent the standard deviation of five biological replicates.

Proteomic Analysis—Multidimensional protein identification technology (MudPIT) was carried out as described previously (40, 41). In brief, proteins from each elution were precipitated with trichloroacetic acid, and the resulting pellets were washed with 100% cold acetone. The dried protein pellets were then resuspended in 8 M urea and reduced and alkylated with tris(2-carboxyethyl)phosphine and chloroacetamide as described previously (42). The proteins were then subjected to proteolytic digestion with LysC overnight at 37 °C with shaking followed by digestion with Trypsin Gold (Promega) after diluting the sample to 2 M urea. The reaction was quenched with formic acid and then pressure-loaded onto a microcapillary column pack with both strong cation exchange resin and reverse phase resin as described previously (42). A nine-step MudPIT run was performed for each sample on an LTQ-Velos Pro that was in-line with a Proxeon Easy nanoLC (41). The resulting RAW data files were processed by protein database matching using SEQUEST within Proteome Discoverer 1.4 (Thermo Fisher Scientific). Database matching was performed using a *Homo sapiens* FASTA database downloaded from UniProt on

03/16/2014. The database also contained potential sample contaminant proteins including human keratins, IgGs, and proteolytic enzymes. The database search was performed with +57 daltons on cysteine as a static modification and the following modifications as dynamic: +16 daltons on methionine (oxidation), +14 daltons on lysine (mono-methylation), +28 daltons on lysine (di-methylation), and +42 daltons on lysine (tri-methylation). All peptide-spectral matches were required to have a false discovery rate of ≤1%. SAINT (significance analysis of interactome) probability scores were calculated as outlined in the CRAPome (contaminant repository for affinity purification) and various previous publications (41, 43–45). Mock purifications were performed in parallel in this study, and analysis was performed using the same methods described above for SAINT analysis.

Results

Enzymatic Inhibition of G9a or Knockdown of WIZ Expression Leads to a Global Reduction in H3K9 Methylation Levels—We initially compared H3K9me2 levels following chemical inhibition of G9a catalytic activity and reduction in G9a protein levels due to *WIZ* knockdown. Inhibition of G9a catalytic activity in HEK293T cells with a small molecule probe, UNC0638 (30), did not result in a change in *G9a*, *GLP*, or *WIZ* mRNA levels (Fig. 1*A*) but did lead to a global reduction in H3K9me2 levels and an increase in G9a protein (Fig. 1, *B* and *C*). Treatment of HEK293T cells with a siRNA against *WIZ* reduced *WIZ* mRNA 5-fold ($p < 0.0001$) but did not affect *G9a* or *GLP* mRNA levels (Fig. 1*D*). H3K9me2 ($p = 0.03$) and WIZ ($p = 0.001$) protein levels decreased compared with the control siRNA (Fig. 1, *E* and *F*). There was also a slight (1.25-fold) decrease in G9a levels, which agrees with a previous study that linked WIZ with G9a protein stability (29). To determine whether *WIZ* knockdown affects long-term G9a protein stability, we stably expressed *WIZ* shRNA or control in a HeLa cell line that expresses a double tagged version of G9a (9). These cells demonstrated no change in *G9a* or *GLP* mRNA levels ($p = 0.1311$), whereas *WIZ* mRNA levels were reduced 2-fold ($p = 0.035$) (Fig. 1*G*). Even after multiple passages of this cell line, the overall change in G9a protein levels remained very small (1.25-fold, $p = 0.02$), whereas H3K9me2 levels were reduced 2.5-fold ($p = 0.01$) and WIZ protein levels were 2.5-fold lower (input, $p = 0.02$) (Fig. 1, *H* and *I*). These data suggest that reduction in H3K9me2 associated with *WIZ* silencing was not due to progressive loss of G9a protein.

WIZ Is Important for G9a Interaction with Chromatin—Because other zinc finger proteins have been shown to regulate lysine methyltransferase activity (46, 47), we investigated the possibility that WIZ is important for G9a retention on chromatin. To assess G9a chromatin interaction, we performed subcellular fractionation of HEK293T cells that were treated with UNC0638, *WIZ* siRNA, or combinations of the two to determine whether these treatments had an additive effect. Neither treatment nor the combination of the two had an effect on *G9a* or *GLP* mRNA levels, whereas *WIZ* mRNA levels were reduced to a similar extent in both the siRNA knockdown and the combination treatment (Fig. 2*A*). H3K9me2 levels were visibly reduced after treatment with UNC0638 in combination with

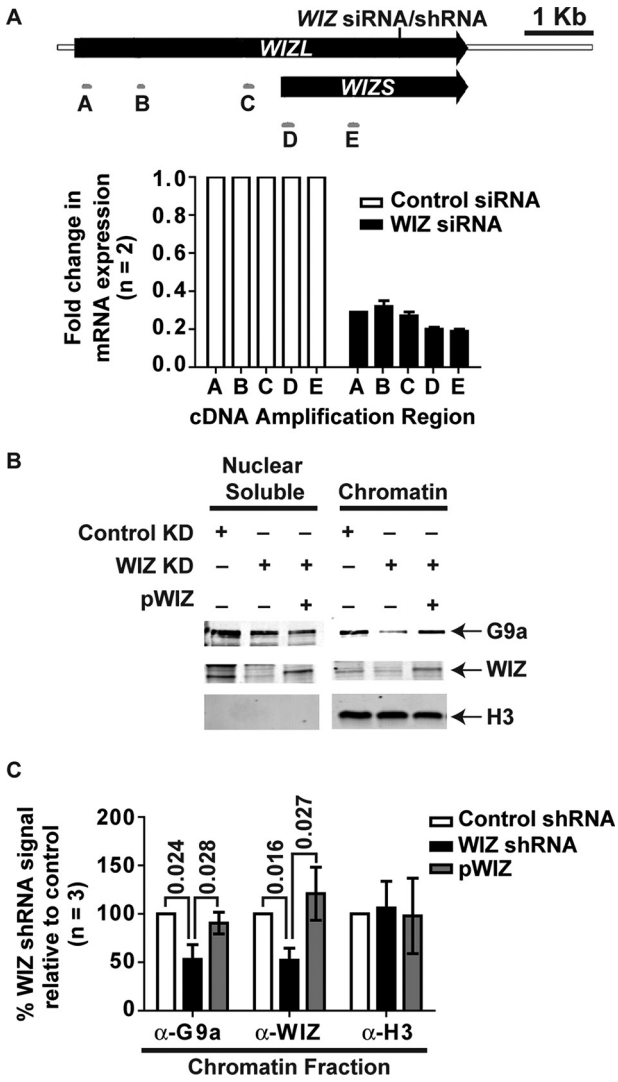

FIGURE 5. **Exogenously expressed *WIZ* restores G9a levels in the chromatin fraction of *WIZ* knockdown cells.** *A*, the open reading frames for the large (*WIZL*) and small (*WIZS*) *WIZ* variants are shown with *black arrows* and the 5′- and 3′-untranslated regions with a *white bar*. *Gray bars* represent qPCR amplicons. The location of *WIZ* siRNA and shRNA is indicated (same sequence targeted). Scale is shown in kb. RT-qPCR showing *WIZ* mRNA levels in HEK293T cells treated with control (*white bars*) or *WIZ* (*black bars*) siRNA for 48 h, normalized to *B2M* mRNA levels. *Error bars* represent the standard error of two biological replicates. *B*, Western blot of nuclear soluble and chromatin fractions from HeLa FLAG-HA-G9a cells stably expressing control or *WIZ* shRNA knockdowns and transiently transfected with a construct expressing human *WIZS* cDNA (*pWIZ*). FLAG-HA-G9a was immunoprecipitated with FLAG-agarose (Sigma). *C*, densitometry of Western bands from the chromatin fraction described for Fig. 4*B*. *Error bars* represent the standard deviation of three biological replicates. The *x* axis shows the antibodies used for Western blotting the chromatin fraction. The *y* axis shows the percent densitometry signal, which was calculated by dividing *WIZ* shRNA or pWIZ band density by the band density for the control shRNA sample. *p* values are indicated.

control siRNA (Fig. 2*B*, compare *lanes 5* and *6*, 4.8-fold) or *WIZ* siRNA (Fig. 2*B*, compare *lanes 5* and *8*, 8.6-fold) and were slightly reduced after treatment with DMSO combined with *WIZ* siRNA (Fig. 2*B*, compare *lanes 5* and *7*, 1.6-fold). Consistent with the changes in H3K9me2 levels, G9a and GLP association with the chromatin fraction was altered after treatment with UNC0638 or *WIZ* siRNA. G9a levels decreased slightly after the addition of UNC0638 (Fig. 2*B*, compare *lanes 5* and *6*, 1.9-fold), *WIZ* siRNA (Fig. 2*B*, compare *lanes 5* and *7*, 1.8-fold),

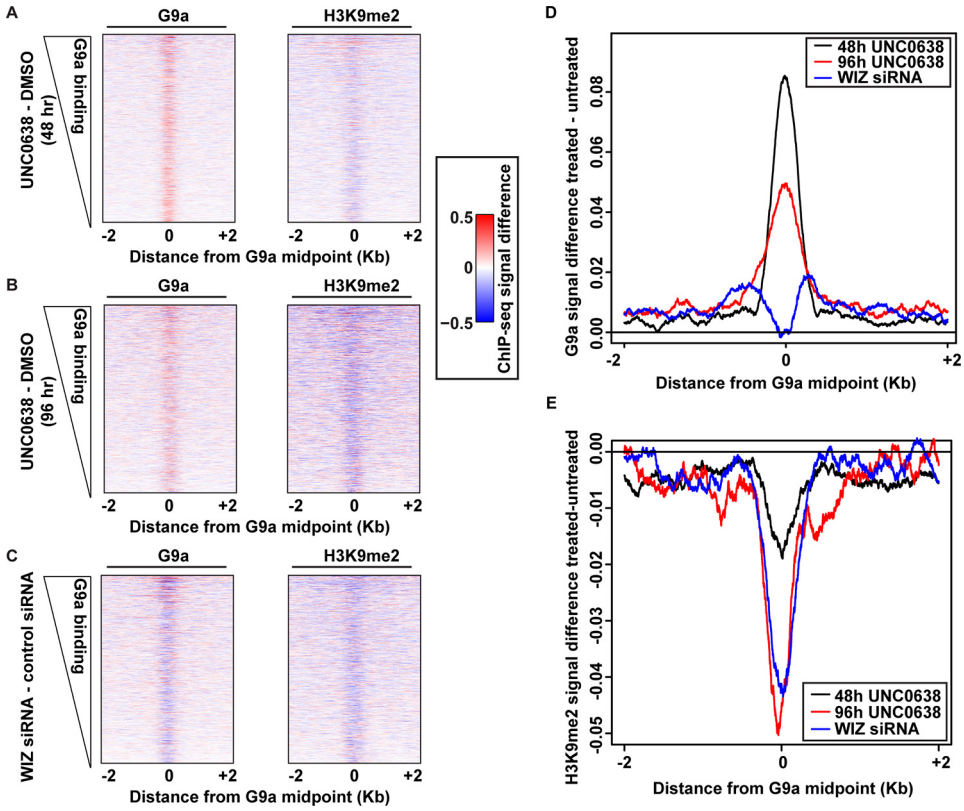

FIGURE 6. **Loss of H3K9me2 signal after *WIZ* siRNA knockdown is due to reduction in G9a occupancy on chromatin.** G9a or H3K9me2 ChIP-seq was performed in HEK293T cells with antibodies against G9a or H3K9me2. Experimental conditions shown are UNC0638 treatment compared with vehicle (DMSO) control at 48 h post-treatment (*A*) and 96 h post-treatment (*B*) and *WIZ* siRNA compared with control knockdown at 72 h post-treatment (*C*). Data are presented as the arithmetic difference between treated and untreated samples after normalization, and color is assigned on a range of −0.5 (*red*) to 0.5 (*blue*). *D*, line plots representing the arithmetic difference in G9a signal between treated and untreated samples after normalization. *E*, line plots representing the arithmetic difference in H3K9me2 signal between treated and untreated samples after normalization. The scales of all *x* axes are shown in kb.

or a combination of both treatments (Fig. 2*B*, compare *lanes 5* and *8*, 6.2-fold). Similar to G9a, GLP levels decreased in the chromatin fraction after the addition of UNC0638 (Fig. 2*B*, compare *lanes 5* and *6*, 1.9-fold), *WIZ* siRNA (Fig. 2*B*, compare *lanes 5* and *7*, 1.7-fold), or a combination of both treatments (Fig. 2*B*, compare *lanes 5* and *8*, 9.1-fold). The dramatic reduction in G9a and GLP protein levels in the chromatin fraction after the combination treatments (Fig. 2*B*, *lane 8*) indicates that enzymatic inhibition and reduction in WIZ protein levels have an additive effect, suggesting that WIZ may help stabilize G9a interaction with chromatin.

Because we observed increased G9a in the soluble fraction after UNC0638 treatment not attributable to an increase in G9a mRNA (Figs. 1*A* and 2*A*), we examined G9a protein stability in HeLa FLAG-HA-G9a cells. We inhibited *de novo* protein synthesis with cycloheximide (CHX) in combination with MG132 proteasome inhibitor, UNC0638, or *WIZ* siRNA knockdown (Fig. 3). Although treatment with UNC0638 for 48 h resulted in higher levels of G9a, none of the treatments demonstrated diminished G9a protein turnover including up to 13.5 h of CHX treatment (Fig. 3*A*). As a control, the levels of a control protein, COXIV, were reduced after 6 h of CHX treatment (Fig. 3*B*). Extending the experiment beyond 13.5 h was not possible (Fig. 3*A*) due to cell toxicity. Thus, we cannot rule out the possibility that UNC0638 increases long-term G9a protein stability.

To further examine G9a association with chromatin, we performed subcellular fractionation of HeLa cells expressing FLAG-HA-tagged G9a followed by FLAG IP of G9a. G9a association with GLP, WIZ, H3K9me3, or H3 did not change following UNC0638 treatment (Fig. 4, *A* and *B*), but H3K9me2 levels in three biological replicate experiments were lower in the input ($p = 0.030$) and IP ($p = 0.001$) samples compared with the H3 input signal (Fig. 4*B*). We repeated the experiment using a FLAG-HA-G9a HeLa stable pool expressing a control or *WIZ* shRNA knockdown (Fig. 4*C*). Although G9a continued to interact with GLP when *WIZ* was knocked down, its interaction with both K9 di-methyl (2.2-fold) and tri-methyl (2.3-fold) H3 and total H3 (2.2-fold) was noticeably reduced. These data indicate that a reduction in WIZ protein levels decreases the association of G9a with histones in the chromatin fraction (Fig. 4*D*). We then examined G9a and WIZ localization to either the nuclear or chromatin fractions (equivalent to Fig. 4, *A* and *C*, *Input*). Treatment with UNC0638 resulted in an increase in G9a protein levels in the nuclear compartment as noted earlier (Fig. 2*B*), but G9a levels remained unchanged in the chromatin fraction, and no alteration in WIZ protein levels was observed (Fig. 4*E*). In contrast, *WIZ* shRNA knockdown significantly reduced G9a levels in the chromatin fraction (Fig. 4*F*, 2-fold).

To confirm that this effect was WIZ-specific, we transfected a plasmid expressing the short human *WIZ* splice variant cDNA into the stable *WIZ* silenced HeLa cells (Fig. 1*E*) followed by subcellular fractionation (Fig. 5). The short isoform (*WIZS*) was selected for reconstitution for several reasons. First, it contains five zinc fingers that are highly conserved in mouse and

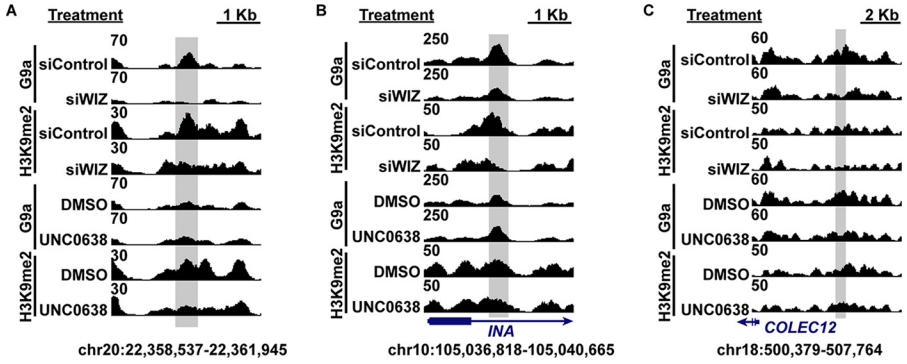

FIGURE 7. **UCSC Genome Browser snapshots of specific genomic regions.** *A–C*, changes in signal are highlighted in *gray*. Occupancy for G9a and H3K9me2 in HEK293T cells is shown in *WIZ* siRNA knockdown (*siWIZ*), control siRNA knockdown (*siNS*), and UNC0638-treated or DMSO-treated cells. A *blue arrow* represents transcribed regions, and the scale is shown in kb in the *top right corner*.

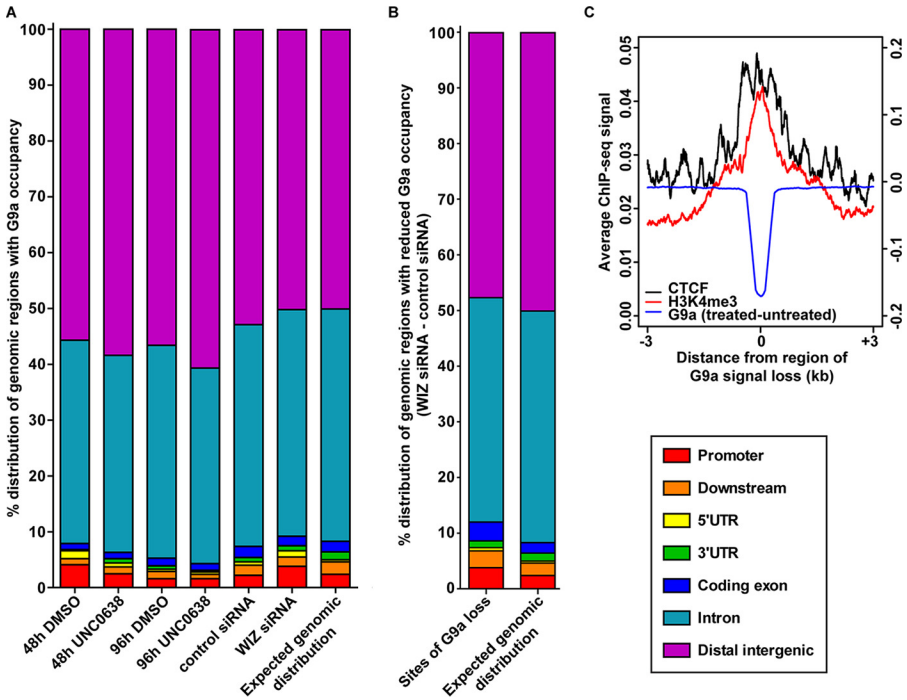

FIGURE 8. **Genomic distribution of G9a.** *A*, the percent distribution of genomic regions with G9a ChIP signal is plotted relative to the genomic coverage of those features. *B*, the percent distribution of regions where G9a signal is lost following *WIZ* siRNA treatment is plotted. *C*, line plot showing the average ChIP signal in HEK293 cells for H3K4me3 (*red line*) and CTCF (*black line*) centered around regions that lose G9a signal after *WIZ* siRNA treatment (*blue line*). Scale is shown in kb. *Left*, *x* axis represents the average ChIP-seq signal for H3K4me3 and CTCF (data from ENCODE). *Right*, *x* axis represents the average ChIP-seq signal for G9a (*WIZ* siRNA − control siRNA signal).

human *WIZ*, whereas the additional zinc fingers present in the long isoform (*WIZL*) are less conserved (26, 48). Second, in mice, *WizL* and *WizS* are expressed at different times during development, with *WizS* being highly expressed in the developing cerebellum and *WizL* expression restricted to the mature cerebellum (26). Despite the disruption of *WizL* in C57BL/6 mice due to the insertion of an ETn retrotransposon, there is no obvious phenotype in the cerebellum, suggesting a nonessential role for *WizL* (48). Third, G9a and GLP interact with the C-terminal zinc finger of WIZ, which is present in the protein product for both splice variants (29). Note that the *WIZ* siRNA recognizes the 3′-end of the *WIZ* transcript, and therefore both isoforms were knocked down after treatment (Fig. 5*A*). Because *WIZ* mRNA was reduced about 2-fold in the shRNA stable cell line (Fig. 1*E*), and the pWIZ vector was overexpressed compared with endogenous *WIZ* (data not shown), we did not mutate the region targeted by *WIZ* shRNA in the pWIZ vector.

In the *WIZ* knockdown pool, G9a protein levels were reduced in the chromatin fraction compared with the control knockdown pool ($p = 0.024$, Fig. 5, *B* and *C*). Transfection of the pWIZ vector resulted in an increase in G9a protein levels in the chromatin fraction to levels comparable with those of the control knockdown pool ($p = 0.028$, Fig. 5, *B* and *C*). Thus, the protein product of the *WIZS* isoform is sufficient to restore G9a and WIZ protein levels to chromatin.

To determine whether G9a chromatin occupancy was affected by enzymatic inhibition or reduced levels of WIZ, we performed chromatin immunoprecipitation followed by high-throughput sequencing (ChIP-seq). HEK293T cells were treated with 1 μM UNC0638 or DMSO for 48 h (Fig. 6*A*) or 96 h

(Fig. 6*B*) or control siRNA or *WIZ* siRNA for 72 h (Fig. 6*C*) followed by ChIP with antibodies against G9a or H3K9me2 (30) (Figs. 6–8).

We first normalized the ChIP-seq enrichment computed over the union set of G9a binding sites to account for differences in the sequencing depth. We then assessed the difference in the G9a and H3K9me2 ChIP-seq signals between UNC0638-treated (Fig. 6, *A* and *B*) or *WIZ* siRNA (Fig. 6*C*)-treated and untreated cells by subtracting the signal from control cells. A reduction in the H3K9me2 signal was observed for all treated samples compared with controls (Fig. 6, *A*–*C* and *E*). Following UNC0638 treatment, the G9a signal was elevated (Fig. 6, *A*, *B*, and *D*), which might be explained by the increase in the G9a protein levels (Figs. 2*B*, 3, and 4*A*). This elevation in the G9a signal was general and subtle, with no one site in the -treated samples having a statistically significant increase over controls. The signal difference decreased and became more diffuse after 96 h. In contrast, *WIZ* siRNA treatment resulted in a loss of G9a signal (Fig. 6, *C* and *D*). Examples of the changes at specific regions are highlighted in Fig. 7. These data suggest that the decreased G9a chromatin binding associated with a reduction in *WIZ* is responsible for the loss of H3K9me2.

Assessment of the genomic distribution of regions with G9a occupancy revealed that the majority of G9a signal was localized to introns or distal intergenic regions (Fig. 8*A*). UNC0638 treatment resulted in a slight increase in G9a occupancy at distal intergenic regions at 48 h (2.8%) and 96 h (4%), with no other large changes in occupancy distribution noted. Treatment with *WIZ* siRNA had little effect on overall G9a distribution, with the remaining G9a signal increasing slightly at promoters (1.6%) and decreasing slightly at distal intergenic regions (2.7%). Because *WIZ* siRNA knockdown resulted in an overall loss of G9a signal, we examined the genomic distribution of regions with reduced G9a occupancy compared with control siRNA knockdown (Fig. 8*B*). We identified 14,116 regions where G9a occupancy was significantly reduced following *WIZ* knockdown (binomial test, $q < 1 \times 10^{-5}$). Many of these differential regions were distal from genes. ~83% of these sites were greater than 10 kilobases (kb) from a transcription start site (TSS), and the median distance to the nearest TSS was ~30 kb. There were, however, 2389 sites within 10 kb of a TSS. Despite the small proportion of sites (~17%) in the vicinity of a TSS, we noted that the loss of G9a was slightly skewed toward promoters and coding exons following *WIZ* siRNA treatment relative to the genomic coverage of those features. By associating the sites of G9a signal loss with ENCODE ChIP data for HEK293 cells (37), we observed signal enrichment with H3K4me3 and the CTCF (Fig. 8*C*), both of which are associated with active transcription.

The Effects on Gene Expression by WIZ Knockdown Do Not Completely Overlap with Those by Enzymatic Inhibition of G9a—Because *WIZ* silencing and G9a inhibition both led to reduced H3K9me2 levels, we asked whether gene expression would be similarly affected. G9a can act as both a co-activator and co-repressor of transcription (49–53). As the ability of G9a to affect transcription is not fully dependent on its catalytic activity, we predicted that treatment with UNC0638 would have a different effect on global gene expression compared with *WIZ* knockdown.

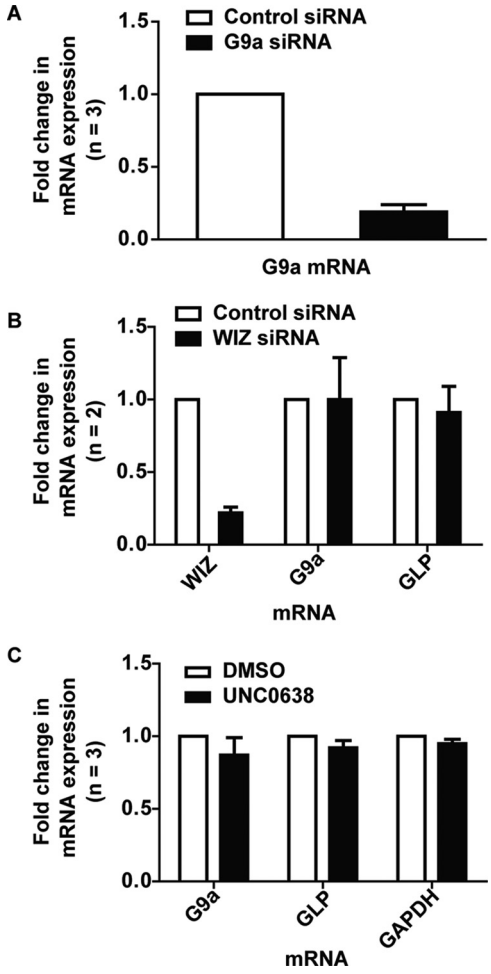

FIGURE 9. **RT-qPCR data from samples used for gene expression microarray analysis.** *A*, RT-qPCR showing *G9a* mRNA levels in HEK293T cells treated with control siRNA (*white bar*) or *G9a* siRNA (*black bar*) for 48 h, normalized to *B2M* mRNA levels. *Error bars* represent the standard deviation of three biological replicates. *B*, RT-qPCR showing indicated transcript levels in HEK293T cells treated with control siRNA (*white bars*) or *WIZ* siRNA (*black bars*) for 48 h, normalized to *B2M* mRNA levels. *Error bars* represent the standard error of two biological replicates. *C*, RT-qPCR showing indicated transcript levels in HEK293T cells treated with DMSO (*white bars*) or UNC0638 (*black bars*) for 48 h, normalized to *B2M* mRNA levels. *Error bars* represent the standard deviation of three biological replicates.

Microarray-based gene expression analysis was performed using cDNA from HEK293T cells treated with *G9a* siRNA, *WIZ* siRNA, or UNC0638 (Fig. 9) and compared with cDNA from control siRNA knockdown or vehicle (DMSO) treatment. We identified genes that demonstrated a concordant (Fig. 10*A*) or divergent (Fig. 10*B*) change in gene expression. Gene expression was median-centered to highlight the magnitude of differential expression.

For genes with a similar trend in RNA abundance after either *WIZ* knockdown or UNC0638 treatment (Fig. 10*A*), 72% (147 of 205 genes at <0.5% false discovery rate) exhibited lower expression, suggesting a significant effect of these treatments on the G9a co-activator function. In comparison, *G9a* knockdown resulted in a 50% overall gene repression (135 of 205 genes). Because the loss of G9a protein results in the degradation of GLP as well as loss of the proteins that would normally interact

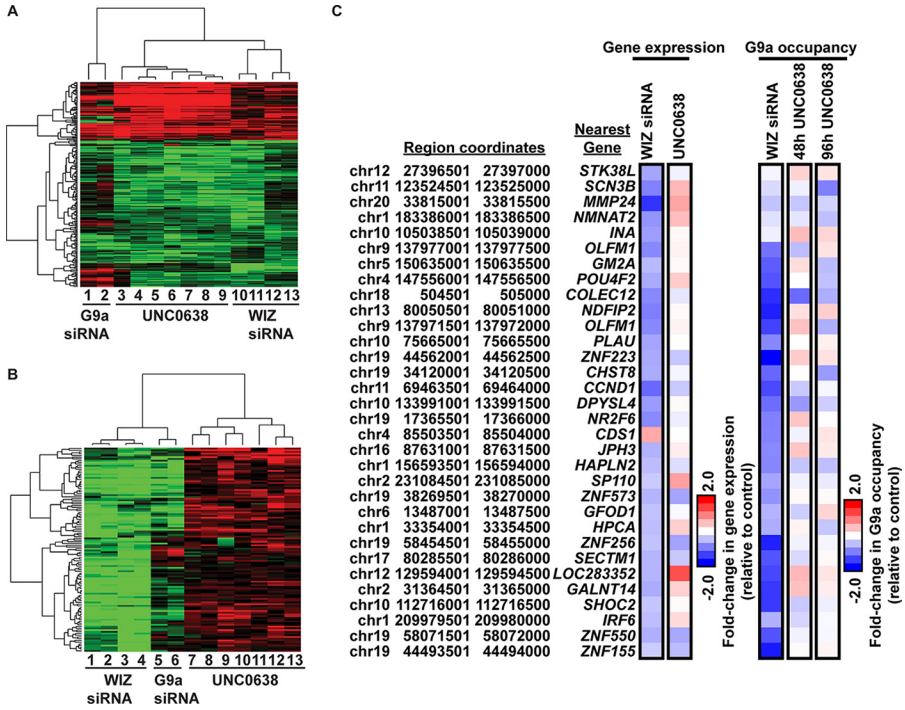

FIGURE 10. **Microarray data indicating that enzymatic inhibition and *WIZ* siRNA knockdown have both overlapping and distinct effects on gene expression.** *A*, heat map of genes with a similar expression pattern relative to control. *Red* indicates genes that have increased expression compared with control, and *green* indicates genes that have decreased expression compared with control. *B*, heat map of differentially expressed genes between HEK293T cells with UNC0638 *versus* *WIZ* siRNA knockdown. Gene expression has been median-centered to highlight the magnitude of differential expression. *Lane numbers* indicate biological replicates. *C*, comparison of gene expression and G9a occupancy. Loss of G9a occupancy in *WIZ* siRNA knockdown HEK293T cells correlates with a reduction in gene expression of a subset of genes (listed as *Nearest Gene*). Gene expression is represented as -fold change in gene expression relative to control from −2.0-fold (*blue*) to 2.0-fold (*red*). G9a occupancy is represented as -fold change in G9a occupancy relative to control from −2.0-fold (*blue*) to 2.0-fold (*red*).

with the heterodimer (13, 25), it is not surprising that *G9a* knockdown affects gene expression differently than either enzymatic inhibition (UNC0638 treatment) or loss of chromatin association (*WIZ* knockdown). Indeed, this observation is also true for genes with divergent expression changes following *WIZ* knockdown *versus* UNC0638 treatment (Fig. 10*B*).

For differentially expressed genes (Fig. 10*B*, 118 genes at <0.5% false discovery rate), enzymatic inhibition resulted in derepression of gene expression, whereas *WIZ* knockdown led to transcriptional repression. As noted earlier, only ~17% of the regions of G9a loss were within 10 kb of a TSS. Of these sites, 42% (or 1015) were near a gene that was represented on our microarray. Although only 32 of those regions were near a gene with a significant ($q < 0.05$) change in gene expression (Fig. 10*C*), all but one of those genes were repressed following *WIZ* knockdown. In contrast, UNC0638 treatment showed less overall change in the gene expression profiles in the same regions. The fact that loss of G9a ChIP signal after *WIZ* knockdown is associated with signals associated with active transcription, but are not generally seen directly at transcription start sites (Fig. 8, *B* and *C*), could indicate that G9a exerts co-transcriptional influence from a distance.

Taken together, these data suggest that binding of G9a to chromatin is important for its role as a co-activator, whereas enzymatic activity is associated with co-repressor function. These observations are consistent with the promoter and exon-skewed loss of G9a following siRNA *WIZ* knockdown (Fig. 8, *B* and *C*) and with prior studies, indicating that G9a catalytic activity is dispensable for co-activator function (49, 50, 52–54).

Enzymatic Inhibition with UNC0638 and WIZ Knockdown Differentially Affect the Interaction of G9a with Its Protein-binding Partners—Based on the observation that WIZ-mediated loss of G9a association with chromatin had different consequences for gene expression compared with enzymatic inhibition, we predicted that G9a protein-protein interactions would also be differentially affected. To determine how enzymatic inhibition of G9a compares with *WIZ* knockdown, FLAG-HA-tagged G9a (9) was tandem affinity-purified from HeLa cells treated with UNC0638 or DMSO (Fig. 11*A*), or cells from the stable control or *WIZ* knockdown pools (Fig. 11*B*), and subjected to mass spectrometry analysis. Significant G9a-associated proteins were determined using the SAINT (44) scoring method (Fig. 12*A*). Both the known and novel associations with prey protein were identified. Enzymatic inhibition of G9a had a greater effect on protein association compared with *WIZ* knockdown (Fig. 12*B*). Differences could be due to the fact that there was only about a 40% reduction in WIZ protein levels in the knockdown cells compared with the control, whereas UNC0638 treatment at 1 μM results in >90% inhibition of catalytic function (30). Alternatively, in the absence of WIZ, G9a may retain catalytic activity toward non-histone substrates.

Discussion

We demonstrated that WIZ is important for G9a interaction with chromatin. Stable knockdown of *WIZ* reduced H3K9me2 levels and resulted in a very slight reduction in G9a protein levels, which remained stable over time (Fig. 1, *G–I*). This WIZ-mediated effect was specific, because reconstitution of exoge-

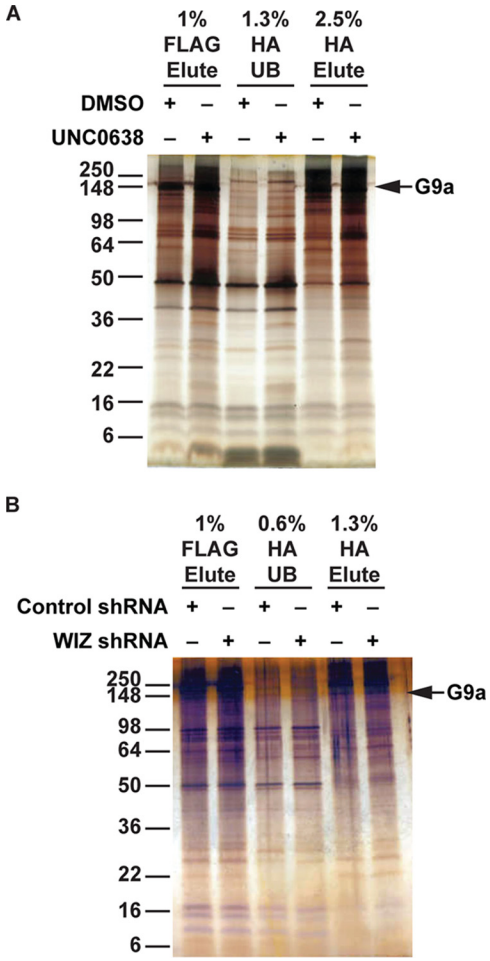

FIGURE 11. **Silver-stained gels showing purified samples submitted for mass spectrometry analysis.** Tandem affinity purification of G9a was performed with FLAG followed by HA. HA elution samples were submitted for mass spectrometry analysis. The FLAG elution (*FLAG Elute*) and HA purification unbound (*HA UB*) samples are shown for reference. *A*, purification from HeLa FLAG-HA-G9a cells treated with DMSO or 1 μM UNC0638 for 48 h. *B*, purification from HeLa FLAG-HA-G9a cells with either control shRNA or *WIZ* shRNA stable knockdown.

nously expressed *WIZ* into *WIZ* knockdown cells increased G9a chromatin-associated protein (Fig. 5, *B* and *C*), and genome-wide, as *WIZ* knockdown resulted in a dramatic loss of G9a occupancy on chromatin (Fig. 6).

The WIZ protein contains C_2H_2-type zinc finger motifs that have an unusually widely spaced configuration (26). In *Petunia*, the EPF family of proteins has two widely separated C_2H_2 zinc fingers that recognize and bind to specific DNA sequences (55–57). *Drosophila* proteins with widely spaced zinc finger motifs include the chromatin-associated suppressor of variegation 3–7 (58–60) and the homeotic protein Teashirt, which binds sequence-specific gene-regulatory sites *in vitro* (61) and behaves as a transcriptional repressor when transfected into human cells (62). The murine orthologues of Teashirt also act as transcriptional repressors and are involved in developmental roles similar to fly Teashirt (63, 64). Thus, despite an unusual configuration, proteins with widely spaced zinc finger motifs are compatible with DNA binding and transcriptional regulation. This conclusion was further supported by findings published while our manuscript was being prepared for submission (65).

Co-transcriptional Activity of G9a—Although both loss of *WIZ* and small molecule inhibition of G9a reduced the H3K9me2 levels, they appeared to do so by distinct mechanisms. UNC0638 binds in the substrate-binding site of G9a and is noncompetitive with the cofactor *S*-adenosyl-L-methionine (30). Yet, although UNC0638 treatment effectively decreased cellular H3K9me2 levels, it did not generally displace G9a from chromatin. In contrast, silencing the G9a complex member *WIZ* resulted in the loss of both H3K9me2 and G9a occupancy on chromatin (Figs. 6 and 7).

The power of a combinatorial approach to the study of G9a signaling was highlighted by differential gene expression analysis, which suggested that G9a catalytic activity was associated with the co-repressor function, whereas G9a occupancy on chromatin was more closely related to its function as a co-activator (Fig. 10*B*). The G9a catalytic domain is sufficient for silencing a target reporter gene (66, 67); however, G9a promotes DNA methylation through its ankyrin repeat domain independently of its lysine methylation activity (13, 68–71). Furthermore, the catalytic activity of G9a is dispensable for transcriptional activation of several genes (49, 50, 52–54), and G9a has a number of non-histone substrates, including itself, which would be affected by enzymatic inhibition but potentially not a knockdown of *WIZ* (17–21). Our results confirmed that catalytic activity was dispensable for the regulation of a subset of genes on our microarray (Fig. 10*B*). A comparison of either UNC0638 treatment or *WIZ* siRNA knockdown to a *G9a* siRNA knockdown would not have revealed this stark contrast, because the loss of G9a produced a gene expression pattern that overlapped with both treatment conditions (Fig 10*B*).

Our ChIP-seq data showed that G9a loss occurred mainly at distal intergenic and intronic regions of the genome (Fig. 8*B*); however, the signal was slightly skewed toward promoters and coding exons. The sites of G9a loss also overlapped with sites of H3K4me3 and CTCF binding (Fig. 8*C*). These data were consistent with our gene expression analysis, which associated G9a occupancy on chromatin with its co-activator activity at a subset of genes (Fig. 10*B*).

Despite the strong association between G9a occupancy and transcriptional activity, we noted that the overall median distance of sites of G9a loss following *WIZ* siRNA knockdown to the nearest TSS was ~30 kb (Fig. 8*B*). In addition, the majority of sites occupied by G9a were located in distal intergenic regions (Fig. 8*A*). These findings suggested that G9a co-transcriptional activity in HEK293T cells was exerted mostly at a significant distance from the site of transcription initiation. The H3K9me2 mark is unique compared with some other histone modifications because of its broad regional deposition (72). It has been proposed that G9a target specificity is determined by multiple interactions with chromatin or sequence-specific DNA-binding molecules (6, 8). It would be interesting to determine whether G9a binding mediates chromatin looping to allow its interaction with multiple sites in the genome from a localized domain.

G9a Protein-interacting Partners—The loss of H3K9me2 by two distinct mechanisms allowed for comparison of the

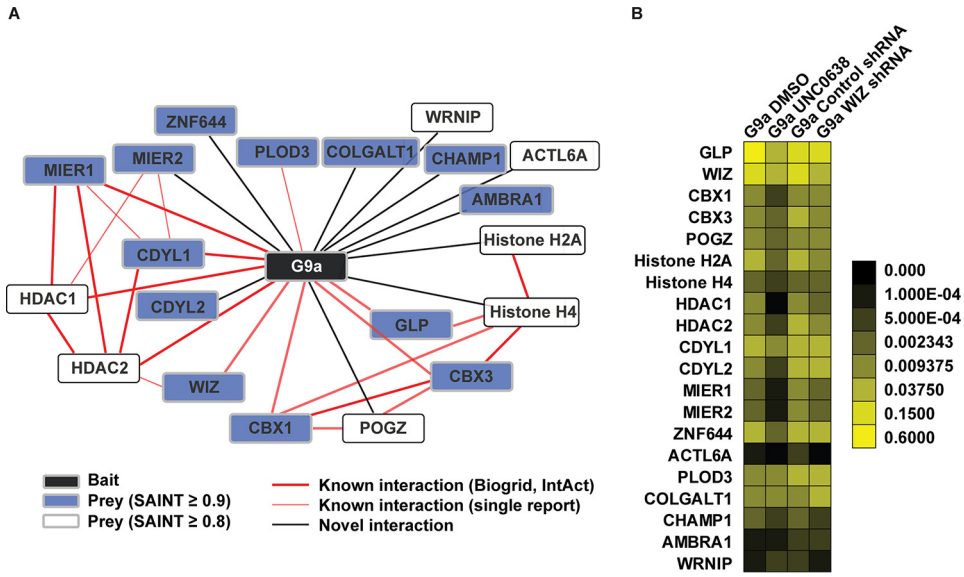

FIGURE 12. **G9a-interacting proteins.** *A*, proteins that interact significantly with G9a. Significantly interacting protein analysis (SAINT) was performed on proteomic data from FLAG-HA-G9a tandem affinity purifications. The *black box* represents the bait protein, G9a; *blue boxes*, SAINT ≥ 0.9; *white boxes*, SAINT ≥ 0.8; *red lines*, known interactions; and *black lines*, novel interactions. *B*, heat map showing changes in normalized spectral abundance factor (NSAF) data from G9a tandem affinity purifications represented in *A*. Treatment conditions are listed at the *top*, and protein names are listed on the *left side*.

genomic and proteomic differences resulting from either enzymatic inhibition or relocalization of G9a. Proteomic data suggested that the interaction of G9a with its non-histone targets was affected by enzymatic inhibition to a greater extent than reduction of WIZ and chromatin targeting (Fig. 12). As expected, GLP and WIZ were identified as significantly interacting proteins (SAINT ≥ 0.9). Additional known G9a-associated proteins include: chromodomain on Y-like 1 (CDYL1) (73, 74), which binds methylated H3K9; histone deacetylase 1 (HDAC1) and HDAC2 (75); mesoderm induction early response 1 (MIER1) (76), which represses transcription through recruitment of HDAC1; and chromobox homologs CBX1 (or heterochromatin protein β (HP1β)) and CBX3 (HP1γ) (77–80), readers of methylated H3K9. Mass spectrometry analysis by others has shown that many of these proteins interact to form complexes. CDYL1 bridges the REST repressor and G9a to regulate neuronal gene expression. In addition to G9a and GLP, CDYL1 co-purified with WIZ, HDAC1 and HDAC2, and MIER1 (81). HDAC2 was shown by mass spectrometry to associate with G9a, GLP, WIZ, MIER1 and MIER2, and the reciprocal purification with G9a bait yielded both HDAC2 and MIER1 (82).

We noted that enzymatic inhibition of G9a had more effect on its protein-interacting partners compared with *WIZ* knockdown (Fig. 12*B*). These data could be the result of an inefficient *WIZ* knockdown (WIZ protein levels were reduced by ~40%), or they could indicate that G9a displaced from chromatin maintains catalytic activity toward non-histone substrates. In support of the latter interpretation, proteins with the greatest abundance of changes in UNC0638-treated cells compared with controls were non-histone substrates or closely associated with non-histone substrates of G9a. Automethylation of G9a has been shown to be important for its interaction with CBX3 (17, 19, 67). Other non-histone substrate protein interactions that are reduced following treatment include CDYL1, HDAC1, GLP, and WIZ (18, 21). Knockdown of *WIZ* did not result in a change in association of G9a with CDYL1 or CDYL2, again implying that G9a enzymatic activity is important for this interaction. Other associations that were affected by enzymatic inhibition, but not *WIZ* knockdown, include CBX1 and ZNF644. These data suggest that methylation of non-histone substrates by G9a could be important for maintaining interactions with various protein complexes.

Overall, our findings underscore the potential of combining small molecule probes with gene silencing to dissect molecular pathways. Understanding the mechanistic basis for differences between pharmacologic and genetic manipulations is essential to any translational hypotheses related to G9a function (83–85).

Author Contributions—S. G. P. conceived and coordinated the study, performed experiments other than those listed below, and wrote the paper. I. J. D. and B. D. S. critically revised the paper. J. M. S. prepared sequencing libraries and analyzed the data shown in Figs. 6–8 and 10*C*. J. S. P. analyzed the data shown in Fig. 10, *A* and *B*. F. L. and J. J. synthesized UNC0638. S. B. R. performed and analyzed experiments shown in Fig. 2*B*. S. A. created the FLAG-HA-G9a HeLa cells lines used throughout the study. A. L. M. performed the mass spectrometry and proteomic analysis shown in Fig. 12. All authors reviewed the results and approved the final version of the manuscript.

Acknowledgments—We thank Dr. S. Frye for helpful advice and editing of the manuscript, Nick Shalosky for large-scale cell culture, and the LCCC Genomics Core for microarray hybridization.

References

1. Black, J. C., Van Rechem, C., and Whetstine, J. R. (2012) Histone lysine methylation dynamics: establishment, regulation, and biological impact. *Mol. Cell* **48,** 491–507
2. Del Rizzo, P. A., and Trievel, R. C. (2014) Molecular basis for substrate

recognition by lysine methyltransferases and demethylases. *Biochim. Biophys. Acta* **1839,** 1404–1415
3. Herz, H. M., Garruss, A., and Shilatifard, A. (2013) SET for life: biochemical activities and biological functions of SET domain-containing proteins. *Trends Biochem. Sci.* **38,** 621–639
4. Rea, S., Eisenhaber, F., O'Carroll, D., Strahl, B. D., Sun, Z. W., Schmid, M., Opravil, S., Mechtler, K., Ponting, C. P., Allis, C. D., and Jenuwein, T. (2000) Regulation of chromatin structure by site-specific histone H3 methyltransferases. *Nature* **406,** 593–599
5. Mozzetta, C., Boyarchuk, E., Pontis, J., and Ait-Si-Ali, S. (2015) Sound of silence: the properties and functions of repressive Lys methyltransferases. *Nature reviews. Mol. Cell Biol.* **16,** 499–513
6. Shankar, S. R., Bahirvani, A. G., Rao, V. K., Bharathy, N., Ow, J. R., and Taneja, R. (2013) G9a, a multipotent regulator of gene expression. *Epigenetics* **8,** 16–22
7. Collins, R., and Cheng, X. (2010) A case study in cross-talk: the histone lysine methyltransferases G9a and GLP. *Nucleic Acids Res.* **38,** 3503–3511
8. Shinkai, Y., and Tachibana, M. (2011) H3K9 methyltransferase G9a and the related molecule GLP. *Genes Dev.* **25,** 781–788
9. Fritsch, L., Robin, P., Mathieu, J. R., Souidi, M., Hinaux, H., Rougeulle, C., Harel-Bellan, A., Ameyar-Zazoua, M., and Ait-Si-Ali, S. (2010) A subset of the histone H3 lysine 9 methyltransferases Suv39h1, G9a, GLP, and SETDB1 participate in a multimeric complex. *Mol. Cell* **37,** 46–56
10. Mozzetta, C., Pontis, J., Fritsch, L., Robin, P., Portoso, M., Proux, C., Margueron, R., and Ait-Si-Ali, S. (2014) The histone H3 lysine 9 methyltransferases G9a and GLP regulate Polycomb repressive complex 2-mediated gene silencing. *Mol. Cell* **53,** 277–289
11. Tachibana, M., Sugimoto, K., Fukushima, T., and Shinkai, Y. (2001) Set domain-containing protein, G9a, is a novel lysine-preferring mammalian histone methyltransferase with hyperactivity and specific selectivity to lysines 9 and 27 of histone H3. *J. Biol. Chem.* **276,** 25309–25317
12. Weiss, T., Hergeth, S., Zeissler, U., Izzo, A., Tropberger, P., Zee, B. M., Dundr, M., Garcia, B. A., Daujat, S., and Schneider, R. (2010) Histone H1 variant-specific lysine methylation by G9a/KMT1C and Glp1/KMT1D. *Epigenetics Chromatin* **3,** 7
13. Tachibana, M., Matsumura, Y., Fukuda, M., Kimura, H., and Shinkai, Y. (2008) G9a/GLP complexes independently mediate H3K9 and DNA methylation to silence transcription. *EMBO J.* **27,** 2681–2690
14. Trojer, P., Zhang, J., Yonezawa, M., Schmidt, A., Zheng, H., Jenuwein, T., and Reinberg, D. (2009) Dynamic histone H1 isotype 4 methylation and demethylation by histone lysine methyltransferase G9a/KMT1C and the Jumonji domain-containing JMJD2/KDM4 proteins. *J. Biol. Chem.* **284,** 8395–8405
15. Wu, H., Chen, X., Xiong, J., Li, Y., Li, H., Ding, X., Liu, S., Chen, S., Gao, S., and Zhu, B. (2011) Histone methyltransferase G9a contributes to H3K27 methylation *in vivo*. *Cell Res.* **21,** 365–367
16. Yu, Y., Song, C., Zhang, Q., DiMaggio, P. A., Garcia, B. A., York, A., Carey, M. F., and Grunstein, M. (2012) Histone H3 lysine 56 methylation regulates DNA replication through its interaction with PCNA. *Mol. Cell* **46,** 7–17
17. Chin, H. G., Estève, P. O., Pradhan, M., Benner, J., Patnaik, D., Carey, M. F., and Pradhan, S. (2007) Automethylation of G9a and its implication in wider substrate specificity and HP1 binding. *Nucleic Acids Res.* **35,** 7313–7323
18. Rathert, P., Dhayalan, A., Murakami, M., Zhang, X., Tamas, R., Jurkowska, R., Komatsu, Y., Shinkai, Y., Cheng, X., and Jeltsch, A. (2008) Protein lysine methyltransferase G9a acts on non-histone targets. *Nat. Chem. Biol.* **4,** 344–346
19. Sampath, S. C., Marazzi, I., Yap, K. L., Sampath, S. C., Krutchinsky, A. N., Mecklenbräuker, I., Viale, A., Rudensky, E., Zhou, M. M., Chait, B. T., and Tarakhovsky, A. (2007) Methylation of a histone mimic within the histone methyltransferase G9a regulates protein complex assembly. *Mol. Cell* **27,** 596–608
20. Huang, J., Dorsey, J., Chuikov, S., Pérez-Burgos, L., Zhang, X., Jenuwein, T., Reinberg, D., and Berger, S. L. (2010) G9a and Glp methylate lysine 373 in the tumor suppressor p53. *J. Biol. Chem.* **285,** 9636–9641
21. Biggar, K. K., and Li, S. S. (2015) Non-histone protein methylation as a regulator of cellular signalling and function. *Nat. Rev. Mol. Cell Biol.* **16,** 5–17
22. Peters, A. H., Kubicek, S., Mechtler, K., O'Sullivan, R. J., Derijck, A. A., Perez-Burgos, L., Kohlmaier, A., Opravil, S., Tachibana, M., Shinkai, Y., Martens, J. H., and Jenuwein, T. (2003) Partitioning and plasticity of repressive histone methylation states in mammalian chromatin. *Mol. Cell* **12,** 1577–1589
23. Jenuwein, T., Laible, G., Dorn, R., and Reuter, G. (1998) SET domain proteins modulate chromatin domains in eu- and heterochromatin. *Cell. Mol. Life Sci.* **54,** 80–93
24. Tachibana, M., Sugimoto, K., Nozaki, M., Ueda, J., Ohta, T., Ohki, M., Fukuda, M., Takeda, N., Niida, H., Kato, H., and Shinkai, Y. (2002) G9a histone methyltransferase plays a dominant role in euchromatic histone H3 lysine 9 methylation and is essential for early embryogenesis. *Genes Dev.* **16,** 1779–1791
25. Tachibana, M., Ueda, J., Fukuda, M., Takeda, N., Ohta, T., Iwanari, H., Sakihama, T., Kodama, T., Hamakubo, T., and Shinkai, Y. (2005) Histone methyltransferases G9a and GLP form heteromeric complexes and are both crucial for methylation of euchromatin at H3-K9. *Genes Dev.* **19,** 815–826
26. Matsumoto, K., Ishii, N., Yoshida, S., Shiosaka, S., Wanaka, A., and Tohyama, M. (1998) Molecular cloning and distinct developmental expression pattern of spliced forms of a novel zinc finger gene *wiz* in the mouse cerebellum. *Brain Res. Mol. Brain Res.* **61,** 179–189
27. Miller, J., McLachlan, A. D., and Klug, A. (1985) Repetitive zinc-binding domains in the protein transcription factor IIIA from *Xenopus* oocytes. *EMBO J.* **4,** 1609–1614
28. Rosenberg, U. B., Schroder, C., Preiss, A., Kienlin, A., Cote, S., Riede, I., and Jackle, H. (1986) Structural homology of the product of the *Drosophila* Kruppel gene with *Xenopus* transcription factor Iiia. *Nature* **319,** 336–339
29. Ueda, J., Tachibana, M., Ikura, T., and Shinkai, Y. (2006) Zinc finger protein Wiz links G9a/GLP histone methyltransferases to the co-repressor molecule CtBP. *J. Biol. Chem.* **281,** 20120–20128
30. Vedadi, M., Barsyte-Lovejoy, D., Liu, F., Rival-Gervier, S., Allali-Hassani, A., Labrie, V., Wigle, T. J., Dimaggio, P. A., Wasney, G. A., Siarheyeva, A., Dong, A., Tempel, W., Wang, S. C., Chen, X., Chau, I., Mangano, T. J., Huang, X. P., Simpson, C. D., Pattenden, S. G., Norris, J. L., Kireev, D. B., Tripathy, A., Edwards, A., Roth, B. L., Janzen, W. P., Garcia, B. A., Petronis, A., Ellis, J., Brown, P. J., Frye, S. V., Arrowsmith, C. H., and Jin, J. (2011) A chemical probe selectively inhibits G9a and GLP methyltransferase activity in cells. *Nat. Chem. Biol.* **7,** 566–574
31. Konze, K. D., Ma, A., Li, F., Barsyte-Lovejoy, D., Parton, T., Macnevin, C. J., Liu, F., Gao, C., Huang, X. P., Kuznetsova, E., Rougie, M., Jiang, A., Pattenden, S. G., Norris, J. L., James, L. I., Roth, B. L., Brown, P. J., Frye, S. V., Arrowsmith, C. H., Hahn, K. M., Wang, G. G., Vedadi, M., and Jin, J. (2013) An orally bioavailable chemical probe of the lysine methyltransferases EZH2 and EZH1. *ACS Chem. Biol.* **8,** 1324–1334
32. Konze, K. D., Pattenden, S. G., Liu, F., Barsyte-Lovejoy, D., Li, F., Simon, J. M., Davis, I. J., Vedadi, M., and Jin, J. (2014) A chemical tool for in vitro and in vivo precipitation of lysine methyltransferase G9a. *ChemMedChem* **9,** 549–553
33. Livak, K. J., and Schmittgen, T. D. (2001) Analysis of relative gene expression data using real-time quantitative PCR and the $2(-\Delta\Delta C(T))$ method. *Methods* **25,** 402–408
34. Lassmann, T., Hayashizaki, Y., and Daub, C. O. (2009) TagDust: a program to eliminate artifacts from next generation sequencing data. *Bioinformatics* **25,** 2839–2840
35. Langmead, B., Trapnell, C., Pop, M., and Salzberg, S. L. (2009) Ultrafast and memory-efficient alignment of short DNA sequences to the human genome. *Genome Biol.* **10,** R25
36. Shin, H., Liu, T., Manrai, A. K., and Liu, X. S. (2009) CEAS: *cis*-regulatory element annotation system. *Bioinformatics* **25,** 2605–2606
37. ENCODE Project Consortium (2012) An integrated encyclopedia of DNA elements in the human genome. *Nature* **489,** 57–74
38. Troyanskaya, O., Cantor, M., Sherlock, G., Brown, P., Hastie, T., Tibshirani, R., Botstein, D., and Altman, R. B. (2001) Missing value estimation methods for DNA microarrays. *Bioinformatics* **17,** 520–525
39. Tusher, V. G., Tibshirani, R., and Chu, G. (2001) Significance analysis of microarrays applied to the ionizing radiation response. *Proc. Natl. Acad.*

Sci. U.S.A. **98,** 5116–5121
40. Mosley, A. L., Hunter, G. O., Sardiu, M. E., Smolle, M., Workman, J. L., Florens, L., and Washburn, M. P. (2013) Quantitative proteomics demonstrates that the RNA polymerase II subunits Rpb4 and Rpb7 dissociate during transcriptional elongation. *Mol. Cell. Proteomics* **12,** 1530–1538
41. Smith-Kinnaman, W. R., Berna, M. J., Hunter, G. O., True, J. D., Hsu, P., Cabello, G. I., Fox, M. J., Varani, G., and Mosley, A. L. (2014) The interactome of the atypical phosphatase Rtr1 in *Saccharomyces cerevisiae*. *Mol. Biosyst.* **10,** 1730–1741
42. Florens, L., and Washburn, M. P. (2006) Proteomic analysis by multidimensional protein identification technology. *Methods Mol. Biol.* **328,** 159–175
43. Choi, H., Liu, G., Mellacheruvu, D., Tyers, M., Gingras, A. C., and Nesvizhskii, A. I. (2012) Analyzing protein-protein interactions from affinity purification-mass spectrometry data with SAINT. *Curr. Protoc. Bioinformatics* **39,** 8.15.1–8.15.23
44. Choi, H., Larsen, B., Lin, Z. Y., Breitkreutz, A., Mellacheruvu, D., Fermin, D., Qin, Z. S., Tyers, M., Gingras, A. C., and Nesvizhskii, A. I. (2011) SAINT: probabilistic scoring of affinity purification-mass spectrometry data. *Nat. Methods* **8,** 70–73
45. Mellacheruvu, D., Wright, Z., Couzens, A. L., Lambert, J. P., St-Denis, N. A., Li, T., Miteva, Y. V., Hauri, S., Sardiu, M. E., Low, T. Y., Halim, V. A., Bagshaw, R. D., Hubner, N. C., Al-Hakim, A., Bouchard, A., Faubert, D., Fermin, D., Dunham, W. H., Goudreault, M., Lin, Z. Y., Badillo, B. G., Pawson, T., Durocher, D., Coulombe, B., Aebersold, R., Superti-Furga, G., Colinge, J., Heck, A. J., Choi, H., Gstaiger, M., Mohammed, S., Cristea, I. M., Bennett, K. L., Washburn, M. P., Raught, B., Ewing, R. M., Gingras, A. C., and Nesvizhskii, A. I. (2013) The CRAPome: a contaminant repository for affinity purification-mass spectrometry data. *Nat. Methods* **10,** 730–736
46. Frietze, S., O'Geen, H., Blahnik, K. R., Jin, V. X., and Farnham, P. J. (2010) ZNF274 recruits the histone methyltransferase SETDB1 to the 3′ ends of ZNF genes. *PLoS ONE* **5,** e15082
47. Maier, V. K., Feeney, C. M., Taylor, J. E., Creech, A. L., Qiao, J. W., Szanto, A., Das, P. P., Chevrier, N., Cifuentes-Rojas, C., Orkin, S. H., Carr, S. A., Jaffe, J. D., Mertins, P., and Lee, J. T. (2015) Functional proteomic analysis of repressive histone methyltransferase complexes PRC2 and G9A reveals ZNF518B as a G9A regulator. *Mol. Cell. Proteomics* **14,** 1435–1446
48. Baust, C., Baillie, G. J., and Mager, D. L. (2002) Insertional polymorphisms of ETn retrotransposons include a disruption of the *wiz* gene in C57BL/6 mice. *Mamm. Genome* **13,** 423–428
49. Chaturvedi, C. P., Hosey, A. M., Palii, C., Perez-Iratxeta, C., Nakatani, Y., Ranish, J. A., Dilworth, F. J., and Brand, M. (2009) Dual role for the methyltransferase G9a in the maintenance of β-globin gene transcription in adult erythroid cells. *Proc. Natl. Acad. Sci. U.S.A.* **106,** 18303–18308
50. Purcell, D. J., Jeong, K. W., Bittencourt, D., Gerke, D. S., and Stallcup, M. R. (2011) A distinct mechanism for coactivator versus corepressor function by histone methyltransferase G9a in transcriptional regulation. *J. Biol. Chem.* **286,** 41963–41971
51. Bittencourt, D., Wu, D. Y., Jeong, K. W., Gerke, D. S., Herviou, L., Ianculescu, I., Chodankar, R., Siegmund, K. D., and Stallcup, M. R. (2012) G9a functions as a molecular scaffold for assembly of transcriptional coactivators on a subset of glucocorticoid receptor target genes. *Proc. Natl. Acad. Sci. U.S.A.* **109,** 19673–19678
52. Lee, D. Y., Northrop, J. P., Kuo, M. H., and Stallcup, M. R. (2006) Histone H3 lysine 9 methyltransferase G9a is a transcriptional coactivator for nuclear receptors. *J. Biol. Chem.* **281,** 8476–8485
53. Oh, S. T., Kim, K. B., Chae, Y. C., Kang, J. Y., Hahn, Y., and Seo, S. B. (2014) H3K9 histone methyltransferase G9a-mediated transcriptional activation of p21. *FEBS Lett.* **588,** 685–691
54. Yuan, X., Feng, W., Imhof, A., Grummt, I., and Zhou, Y. (2007) Activation of RNA polymerase I transcription by cockayne syndrome group B protein and histone methyltransferase G9a. *Mol. Cell* **27,** 585–595
55. Takatsuji, H., and Matsumoto, T. (1996) Target-sequence recognition by separate-type Cys2/His2 zinc finger proteins in plants. *J. Biol. Chem.* **271,** 23368–23373
56. Takatsuji, H., Mori, M., Benfey, P. N., Ren, L., and Chua, N. H. (1992) Characterization of a zinc finger DNA-binding protein expressed specifically in petunia petals and seedlings. *EMBO J.* **11,** 241–249
57. Takatsuji, H., Nakamura, N., and Katsumoto, Y. (1994) A new family of zinc finger proteins in petunia: structure, DNA sequence recognition, and floral organ-specific expression. *Plant Cell* **6,** 947–958
58. Cléard, F., Delattre, M., and Spierer, P. (1997) SU(VAR)3–7, a *Drosophila* heterochromatin-associated protein and companion of HP1 in the genomic silencing of position-effect variegation. *EMBO J.* **16,** 5280–5288
59. Cléard, F., Matsarskaia, M., and Spierer, P. (1995) The modifier of position-effect variegation Suvar(3)7 of *Drosophila*: there are two alternative transcripts and seven scattered zinc fingers, each preceded by a tryptophan box. *Nucleic Acids Res.* **23,** 796–802
60. Reuter, G., Giarre, M., Farah, J., Gausz, J., Spierer, A., and Spierer, P. (1990) Dependence of position-effect variegation in *Drosophila* on dose of a gene encoding an unusual zinc-finger protein. *Nature* **344,** 219–223
61. Alexandre, E., Graba, Y., Fasano, L., Gallet, A., Perrin, L., De Zulueta, P., Pradel, J., Kerridge, S., and Jacq, B. (1996) The *Drosophila* Teashirt homeotic protein is a DNA-binding protein and modulo, a HOM-C regulated modifier of variegation, is a likely candidate for being a direct target gene. *Mech. Dev.* **59,** 191–204
62. Waltzer, L., Vandel, L., and Bienz, M. (2001) Teashirt is required for transcriptional repression mediated by high Wingless levels. *EMBO J.* **20,** 137–145
63. Caubit, X., Coré, N., Boned, A., Kerridge, S., Djabali, M., and Fasano, L. (2000) Vertebrate orthologues of the *Drosophila* region-specific patterning gene *teashirt*. *Mech. Dev.* **91,** 445–448
64. Manfroid, I., Caubit, X., Kerridge, S., and Fasano, L. (2004) Three putative murine Teashirt orthologues specify trunk structures in *Drosophila* in the same way as the *Drosophila* teashirt gene. *Development* **131,** 1065–1073
65. Bian, C., Chen, Q., and Yu, X. (2015) The zinc finger proteins ZNF644 and WIZ regulate the G9a/GLP complex for gene repression. *eLife* **4,** eLife.05606; Correction (2015) The zinc finger proteins ZNF644 and WIZ regulate the G9a/GLP complex for gene repression. *eLife* **4,** eLife.08168
66. Snowden, A. W., Gregory, P. D., Case, C. C., and Pabo, C. O. (2002) Gene-specific targeting of H3K9 methylation is sufficient for initiating repression *in vivo*. *Curr. Biol.* **12,** 2159–2166
67. Stewart, M. D., Li, J., and Wong, J. (2005) Relationship between histone H3 lysine 9 methylation, transcription repression, and heterochromatin protein 1 recruitment. *Mol. Cell. Biol.* **25,** 2525–2538
68. Dong, K. B., Maksakova, I. A., Mohn, F., Leung, D., Appanah, R., Lee, S., Yang, H. W., Lam, L. L., Mager, D. L., Schübeler, D., Tachibana, M., Shinkai, Y., and Lorincz, M. C. (2008) DNA methylation in ES cells requires the lysine methyltransferase G9a but not its catalytic activity. *EMBO J.* **27,** 2691–2701
69. Epsztejn-Litman, S., Feldman, N., Abu-Remaileh, M., Shufaro, Y., Gerson, A., Ueda, J., Deplus, R., Fuks, F., Shinkai, Y., Cedar, H., and Bergman, Y. (2008) *De novo* DNA methylation promoted by G9a prevents reprogramming of embryonically silenced genes. *Nat. Struct. Mol. Biol.* **15,** 1176–1183
70. Bittencourt, D., Lee, B. H., Gao, L., Gerke, D. S., and Stallcup, M. R. (2014) Role of distinct surfaces of the G9a ankyrin repeat domain in histone and DNA methylation during embryonic stem cell self-renewal and differentiation. *Epigenetics Chromatin* **7,** 27
71. Collins, R. E., Northrop, J. P., Horton, J. R., Lee, D. Y., Zhang, X., Stallcup, M. R., and Cheng, X. (2008) The ankyrin repeats of G9a and GLP histone methyltransferases are mono- and dimethyllysine binding modules. *Nat. Struct. Mol. Biol.* **15,** 245–250
72. Wen, B., Wu, H., Shinkai, Y., Irizarry, R. A., and Feinberg, A. P. (2009) Large histone H3 lysine 9 dimethylated chromatin blocks distinguish differentiated from embryonic stem cells. *Nat. Genet.* **41,** 246–250
73. Caron, C., Pivot-Pajot, C., van Grunsven, L. A., Col, E., Lestrat, C., Rousseaux, S., and Khochbin, S. (2003) Cdyl: a new transcriptional co-repressor. *EMBO Rep.* **4,** 877–882
74. Lahn, B. T., Tang, Z. L., Zhou, J., Barndt, R. J., Parvinen, M., Allis, C. D., and Page, D. C. (2002) Previously uncharacterized histone acetyltransferases implicated in mammalian spermatogenesis. *Proc. Natl. Acad. Sci. U.S.A.* **99,** 8707–8712
75. Taunton, J., Hassig, C. A., and Schreiber, S. L. (1996) A mammalian histone deacetylase related to the yeast transcriptional regulator Rpd3p. *Sci-*

ence **272,** 408–411
76. Ding, Z., Gillespie, L. L., and Paterno, G. D. (2003) Human MI-ER1 α and β function as transcriptional repressors by recruitment of histone deacetylase 1 to their conserved ELM2 domain. *Mol. Cell. Biol.* **23,** 250–258
77. Eissenberg, J. C., James, T. C., Foster-Hartnett, D. M., Hartnett, T., Ngan, V., and Elgin, S. C. (1990) Mutation in a heterochromatin-specific chromosomal protein is associated with suppression of position-effect variegation in *Drosophila melanogaster*. *Proc. Natl. Acad. Sci. U.S.A.* **87,** 9923–9927
78. James, T. C., and Elgin, S. C. (1986) Identification of a nonhistone chromosomal protein associated with heterochromatin in *Drosophila melanogaster* and its gene. *Mol. Cell. Biol.* **6,** 3862–3872
79. Saunders, W. S., Chue, C., Goebl, M., Craig, C., Clark, R. F., Powers, J. A., Eissenberg, J. C., Elgin, S. C., Rothfield, N. F., and Earnshaw, W. C. (1993) Molecular cloning of a human homologue of *Drosophila* heterochromatin protein HP1 using anti-centromere autoantibodies with anti-chromo specificity. *J. Cell Sci.* **104,** 573–582
80. Singh, P. B., Miller, J. R., Pearce, J., Kothary, R., Burton, R. D., Paro, R., James, T. C., and Gaunt, S. J. (1991) A sequence motif found in a *Drosophila* heterochromatin protein is conserved in animals and plants. *Nucleic Acids Res.* **19,** 789–794
81. Mulligan, P., Westbrook, T. F., Ottinger, M., Pavlova, N., Chang, B., Macia, E., Shi, Y. J., Barretina, J., Liu, J., Howley, P. M., Elledge, S. J., and Shi, Y. (2008) CDYL bridges REST and histone methyltransferases for gene repression and suppression of cellular transformation. *Mol. Cell* **32,** 718–726
82. Bantscheff, M., Hopf, C., Savitski, M. M., Dittmann, A., Grandi, P., Michon, A. M., Schlegl, J., Abraham, Y., Becher, I., Bergamini, G., Boesche, M., Delling, M., Dümpelfeld, B., Eberhard, D., Huthmacher, C., Mathieson, T., Poeckel, D., Reader, V., Strunk, K., Sweetman, G., Kruse, U., Neubauer, G., Ramsden, N. G., and Drewes, G. (2011) Chemoproteomics profiling of HDAC inhibitors reveals selective targeting of HDAC complexes. *Nat. Biotechnol.* **29,** 255–265
83. Bunnage, M. E., Chekler, E. L., and Jones, L. H. (2013) Target validation using chemical probes. *Nat. Chem. Biol.* **9,** 195–199
84. Weiss, W. A., Taylor, S. S., and Shokat, K. M. (2007) Recognizing and exploiting differences between RNAi and small-molecule inhibitors. *Nat. Chem. Biol.* **3,** 739–744
85. Cole, P. A. (2008) Chemical probes for histone-modifying enzymes. *Nat. Chem. Biol.* **4,** 590–597